ORIGINAL ARTICLES

PHOTO-INDUCED PROCESSES OF IRON OXIDE NANOPARTICLES TO ENHANCE LASER THERAPY

Pominova D.V.[1,2], Romanishkin I.D.[1], Plotnikova E.A.[3], Morozova N.B.[3], Loschenov V.B.[1,2], Wittig R.[4], Linden M.[5], Steiner R.W.[2], Ryabova A.V.[1,2]
[1]Prokhorov General Physics Institute of the Russian Academy of Sciences, Moscow, Russia
[2]National Research Nuclear University «MEPhI», Moscow, Russia
[3]P.A. Herzen Moscow Oncology Research Center – branch of FSBI NMRRC of the Ministry of Health of the Russian Federation, Moscow, Russia
[4]Institute for Laser Technologies in Medicine & Metrology, Ulm, Germany
[5]Institute for Inorganic Chemistry II at Ulm University, Ulm, Germany

Abstract

Nanoparticles are used as drug carriers to increase the selectivity and effectiveness of therapy, as well as for combined therapy that utilizes different effects. Iron oxide nanoparticles are promising in this aspect. Due to magnetic properties, they can be used as a contrast agent for magnetic resonance imaging. Also, iron oxide nanoparticles could be coated with a photosensitizer for photodynamic therapy and their laser or magnetic heating can be used for phototherapy. Local enhancement of the electromagnetic field near iron oxide nanoparticles can increase the fluorescence intensity of photosensitizers and the efficiency of singlet oxygen generation.

This paper presents the results of a study of iron oxide nanoparticles focused on the photophysical aspects of the formation of "hot spots" under laser irradiation. The photoinduced effects of iron oxide nanoparticles observed in *in vitro* experiments lead to the rupture of lysosomes. Theoretical modeling showed that the heating of iron oxide nanoparticles with a radius of 35 nm under the action of laser radiation is about 89°C and 19°C for wavelengths of 458 and 561 nm, respectively. Local field enhancement occurs in pairs of nanoparticles of various sizes and strongly depends on the distance between them. The maximum gain is achieved at small distances between nanoparticles. For a dimer of nanoparticles with radii of 10 and 35 nm at a distance of 1 nm, an enhancement factor of two orders of magnitude was obtained. The investigated phenomenon of «hot spots» is in demand for precision therapy, because the photo-induced processes occur at small distances between nanoparticles, in areas of their high accumulation.

Keywords: Iron oxide nanoparticles, plasmon polaritons, «hot spots», modeling, laser hyperthermia, electromagnetic field amplification.

For citations: Pominova D.V., Romanishkin I.D., Plotnikova E.A., Morozova N.B., Loschenov V.B., Wittig R., Linden M., Steiner R.W., Ryabova A.V. Photo-induced processes of iron oxide nanoparticles to enhance laser therapy, *Biomedical Photonics*, 2021, vol. 10, no. 4, pp. 44–58. doi: 10.24931/2413–9432–2021–10-4-44-58

Contacts: Ryabova A.V., e-mail: nastya.ryabova@gmail.com

ФОТОИНДУЦИРОВАННЫЕ ПРОЦЕССЫ НАНОЧАСТИЦ ОКСИДА ЖЕЛЕЗА ДЛЯ УСИЛЕНИЯ ЛАЗЕРНОЙ ТЕРАПИИ

Д.В. Поминова[1,2], И.Д. Романишкин[1], Е.А. Плотникова[3], Н.Б. Морозова[3], В.Б. Лощенов[1,2], R. Wittig[4], M. Linden[5], R.W. Steiner[2], А.В. Рябова[1,2]
[1]Институт общей физики им. А.М. Прохорова Российской академии наук, Москва, Россия
[2]Национальный исследовательский ядерный университет «МИФИ», Москва, Россия
[3]Московский научно-исследовательский онкологический институт им. П.А. Герцена – филиал ФГБУ «Национальный медицинский исследовательский центр радиологии» Министерства здравоохранения Российской Федерации, Москва, Россия
[4]Институт лазерных технологий в медицине и метрологии, Ульм, Германия
[5]Институт неорганической химии II Университета г. Ульм, Ульм, Германия

Резюме

Наночастицы используются в качестве носителей лекарственных средств для повышения селективности и эффективности терапии, а также для сочетанной терапии, объединяющей разные виды воздействия. Перспективными в этом аспекте являются наночастицы оксида железа. Благодаря магнитным свойствам, они могут быть применяться в качестве контраста для магнитно-резонансной томографии. Также наночастицы оксида железа могут быть покрыты фотосенсибилизатором для фотодинамической терапии, а их лазерный или магнитный нагрев этих частиц может используется для проведения фототерапии. При этом локальное усиление электромагнитного поля вблизи наночастиц оксида железа может повысить интенсивность флуоресценции фотосенсибилизаторов и эффективность генерации синглетного кислорода.

В работе представлены результаты исследования наночастиц оксида железа, сфокусированного на фотофизических аспектах образования «горячих точек» при лазерном облучении. Фотоиндуцированные эффекты наночастиц оксида железа, наблюдаемые в экспериментах *in vitro*, приводят к разрыву лизосом. Теоретическое моделирование показало, что нагрев наночастиц оксида железа радиусом 35 нм под действием лазерного излучения составляет порядка 89°C и 19°C для длин волн 458 и 561 нм, соответственно. Локальное усиление поля возникает в парах из наночастиц различного размера и сильно зависит от расстояния между ними. Максимальное усиление достигается при малых расстояниях между наночастицами. Для димера наночастиц с радиусами 10 нм и 35 нм на расстоянии 1 нм получен фактор усиления на два порядка. Рассмотренное явление «горячих точек» востребовано для прецизионной терапии, так как фотоиндуцированные процессы возникают на малых расстояниях между наночастицами, в областях с их высоким накоплением.

Ключевые слова: наночастицы оксида железа, плазмон-поляритоны, «горячие точки», моделирование, лазерная гипертермия, усиление электромагнитного поля.

Для цитирования: Поминова Д.В., Романишкин И.Д., Плотникова Е.А., Морозова Н.Б., Лощенов В.Б., Wittig R., Linden M., Steiner R.W., Рябова А.В. Фотоиндуцированные процессы наночастиц оксида железа для усиления лазерной терапии // Biomedical Photonics. – 2021. – Т. 10, № 4. – С. 44–58. doi: 10.24931/2413–9432–2021–10-4-44-58

Контакты: Рябова А.В., e-mail: nastya.ryabova@gmail.com

Introduction

Nanoparticles (NPs) are attracting great attention due to the recent progress in their synthesis and surface functionalization, along with their ability of photothermal conversion [1] and fluorescence in the near infrared region [2]. The photothermal conversion produces heating and leads to the formation of reactive oxygen species, which destroy cancer cells [3]. NPs can become an ideal drug carrier when modified for vector delivery and controlled release [4].

Hyperthermia is an attractive physical approach for cancer treatment [5-8]. When the tissue temperature rises, usually to 40–45 °C, blood flow and tissue oxidation increase [9], collagen fibers weaken [10], and tumors become more sensitive to chemotherapy drugs [11, 12] or radiation [13-14]. Currently, there are various clinical approaches that use special probes and needles to generate heat using microwaves, radiofrequencies or ultrasound [15, 16], but they do not allow local heating of the targeted pathological areas.

Iron oxide exhibits amazing physical properties, especially in the nanometer range. Iron oxide NPs (IONPs) can be used for magnetic resonance imaging (MRI) / optical multimodal imaging, as well as a therapeutic mediator in the treatment of cancer [17]. IONPs themselves show promising preclinical results in cancer therapy by modulating tumor-associated macrophages [18]. Recently, data were published on the therapeutic effect of Ferumoxytol — suppression of cancer cells and activation of the immune response to tumor [19]. IONPs have low cytotoxicity [20], and their coating with silicon dioxide further reduces both histo- and cytotoxicity [21, 22].

To localize the process of laser hyperthermia, thermal sensitizers like magnetic or plasmon resonance NPs are increasingly used [23]. Ultra small (about 30 nm in size) superparamagnetic IONPs (SPIO) can effectively inhibit tumor progression as photothermal agents [24]. The SPIO heat dissipation mechanism is closely related to dipole-dipole interactions in an alternating magnetic field. For a mixture of IONPs colloids with different sizes, the possibility of simultaneously creating several types of "hot spots" by varying the parameters of the magnetic field has been demonstrated [25]. Thus, the local temperature rise, measured by fluorescent proteins on the surface of IONPs, reached 85 °C. Superparamagnetic particles dissipate heat due to the Néel-Brown relaxation [26, 27]. In magnetic hyperthermia, intracellular aggregation of IONPs inside endosomes is recognized as an important problem, because both physical mechanisms are suppressed: Brownian relaxation of nanoparticles —rotation of whole magnetic nanoparticles in their environment, and Néel relaxation, or rotation of the magnetic moment inside magnetic circuits [28]. Additional disadvantage of the clinical use of magnetic hyperthermia is the need for high concentrations of IONPs, [Fe]=1–2 M, several orders of magnitude higher than the concentrations used for MRI [29]. Efforts are being made to optimize the heating efficiency of the IONPs [30, 31].

More recently, IONPs have been tested for *in vitro* and *in vivo* photothermal therapy. The use of iron oxide nanocubes as sensors for both magnetic and laser hyperthermia has shown high efficiency of hyperthermia in mouse tumor models [32]. The effect of laser hyperthermia has also been demonstrated on magnetic IONPs coated with infrared (IR) dyes Cyanine7 [33] and IR-780 [34]. It was noted that intracellular aggregation of IONPs leads to some increase in the photothermal heating of nanoparticles [35]. There are also reports about the successful use of IONPs in combination with photosensitizers for photodynamic therapy [36,37].

When laser radiation interacts with nanoparticles, light is absorbed and heat is scattered. The study of these processes forms the currently actively developing area of called thermoplasmonics [38]. The interaction of an incident wave with a NP can be characterized using the scattering and absorption cross sections of NPs. The scattering cross section characterizes the part of the radiation that, after interacting with the NP, is scattered in different direction. The absorption cross section describes the energy absorbed by the NP. However, the absorption and scattering cross sections do not in any way characterize the processes occurring in NPs in the plasmon resonance region [39]. It was shown that in the region of plasmon resonance, the energy flux lines form vortex structures around the nanoparticle, which explains the increase in the absorption cross section of nanoparticles compared to the geometric cross section: due to the formation of vortex structures, the energy flux lines pass through the particle several times, which enhances the interaction between light and the material.

The heating that occurs when light interacts with nanomaterials can have different physical mechanisms, which depend on the nature of the nanomaterial. The absorption of photons usually leads to the excitation of photocarriers into excited states determined by quantum mechanics, and their return to the ground state is regulated by radiative (i.e. emission of photons) or nonradiative processes. The latter are associated with photonic, charge, or spin excitations or processes of photocarrier tunneling between defect / impurity electronic states, when the transition energy is very low. At the nanoscale, nonradiative processes lead to highly efficient photothermal conversion processes in which absorbed optical energy is dissipated into heat.

In semiconducting materials such as iron oxides, the energy of optical radiation allows for a temporary transition of electrons from the valence band to the conduction band, which leads to the release of heat with the electrons relaxation back to the valence band [40]. Photothermal conversion of non-metallic inorganic nanoparticles demonstrates moderate efficiency and broader optical absorption than of their metallic counterparts. Interestingly, diffuse and direct optical transmission and reflection components play an important role in the absorption / scattering of photons by colloids, especially when IONPs are aggregated [41].

In plasmon-resonant NPs, a localized surface exciton creates a high-intensity localized electromagnetic (EM) field near the surface, which has a significant effect on the probability of optical processes, such as absorption and radiative transitions (Purcell effect) [42]. An increase in the electric field strength between two gold nanoparticles of different sizes by two to three orders of magnitude is well described in the literature. However, similar phenomena for dielectric nanoparticles, such as iron oxide nanoparticles, are poorly studied. Large resonant field increases were predicted in the gap (from 1 to 30 nm) between two dielectric silicon microdiscs [43].

According to our experimental data, when studying the accumulation of iron oxide nanoparticles in cells using laser scanning microscopy, bright sparks or "hot spots" were observed in the images. As shown in *in vitro* experiments, the emergence of "hot spots" between IONPs during laser irradiation leads to cell death. Presumably, the emergence of "hot spots" and the enhancement of the therapeutic effect may be associated with an increase in the EM field between several IONPs, by analogy with metal NPs [44], or their heating. In this work, we performed theoretical modeling of the EM field enhancement for individual IONPs and their dimers.

Materials and methods

We used commercially available NPs of iron oxide Fe_2O_3 (IONPs) obtained by gas-phase condensation (NanoArc® by AlfaAesar®, USA), particle size 20–70 nm, surface area 30–60 m^2/g, γ-phase.

Sizing and Spectral Characterization of IONPs

The size and morphology of IONPs were analyzed by transmission electron microscopy (TEM) using a LEO 912 AB Omega microscope (Carl Zeiss Group, Germany). The hydrodynamic sizes of NPs and the ζ-potential were determined using a Zetasizer Nano ZS (Malvern Instruments, UK) in dH_2O at 25 °C. All measurements were triplicated. The absorption of colloids IONPs in the 0.4–0.8 μm spectral range was studied using a Hitachi U-3400 spectrophotometer (Hitachi Ltd., Japan). The absorbance was measured in cuvettes with an optical path length of 1 cm; the mass concentration of IONPs was 0.02 mg/mL.

"Hot spot" detection

To detect "hot spots" under laser irradiation, a laser scanning confocal microscope LSM-710 (Carl Zeiss,

Germany) was used. For measurements, the samples were placed between two cover glasses with a fixed distance determined by the thickness of the silicone spacer between them. Scanning was performed with lasers with 488 and 561 nm wavelengths. The laser power at the exit from the objective was determined using a LabMax-TO laser power meter (Coherent, USA).

The intensity distribution of the scanning laser spot was calculated from considerations of the size of the area bounded by the first-order diffraction ring for the PSF_{ill} point (or Airy disk) distribution function, with radius r:

$$r = \frac{0.61\lambda_{\mathbf{exc}}}{NA}, (1)$$

where *NA* is the numerical aperture of the microscope objective, λ_{exc} is the excitation wavelength.

For a 458 nm laser and a 63× oil objective with NA = 1.4, r = 200 nm, spot area S = 0.13 μm^2, measured power density at the lens exit = 1 mW, scanning power density ρ = 0.839 * P/S = 0.668 MW/cm^2, at a scanning speed of 0.53 μs/pixel (for temperature measurements) and 1.62 μs/pixel (for cells), the radiation dose for a single scan A = ρ×t was 0.35 J/cm^2 (for temperature measurements) and 1.08 J/cm^2 (for cells).

For a 561 nm laser, 63× oil objective with NA = 1.4, r = 244 nm, spot area S = 0.19 μm^2, measured power density at the objective exit = 1 mW, scanning power density ρ = 0.445 MW/cm^2, at a scanning speed of 0.53 μs/pixel (for temperature measurements) and 1.62 μs/pixel (for cells), the radiation dose in a single scan was 0.24 J/cm^2 (for temperature measurements) and 0.72 J/cm^2 (for cells).

The dependence of the "hot spots" number on the concentration of IONPs, as well as on the ambient temperature, was studied. For this, two colloids were prepared with IONPs concentrations of 0.1 and 0.01 mg/L. To study the effect of heating on the "hot spots" number, the studied samples were heated on the microscope thermostat (PeCon GmbH, Erbach, Germany) in the 20–60 °C temperature range.

The "hot spots" spectra were also studied using the laser scanning microscope. The emission spectra of "hot spots" were recorded with a 32-channel GaAsP detector in the 400–750 nm spectral range. Each "hot spot" was visualized by a microscope as a group of several pixels with different brightness. At the initial moment of time, which corresponds to the first pixel, the brightness is low. Then there is a flare-up to maximum brightness, after which the brightness decreases again. To obtain the resulting spectrum, averaging was carried out for several "hot spots" over pixels with the same step after the occurrence, i.e. with approximately the same brightness.

Registration of "hot spots" in cells in vitro

The intracellular distribution of IONPs and laser-induced "hot spots" were studied in HeLa cell culture. HeLa cells were cultured in RPMI-1640 medium containing 10% fetal calf serum at 37°C in 5% CO_2. The cells were subcultured every third day. For confocal microscopy, cells were plated onto a Petri dish with a glass bottom POC-R2 (PeCon GmbH, Erbach, Germany) at a density of 100 × 10^3 /cm^2 one day before the experiment. The next day, IONPs were added to the cells 4 hours before the start of microscopic examination. Before microscopic examination, cells were washed twice with pre-warmed phosphate buffered saline.

Theoretical modeling of the spectroscopic properties of IONPs

We simulated the scattering and absorption cross sections of individual IONPs in water, as well as local field enhancement near individual IONPs and between two nanoparticles of different sizes, forming a dimer. Water was used as the surrounding dielectric medium in the model.

The optical properties of individual spherical IONPs with a radius of 10 and 35 nm in the near and far fields were simulated using the T-matrix method [45, 46]. The scattering was calculated for the 400-800 nm optical wavelength range. The complex refractive indices of gold and iron oxide were taken from https://refractiveindex.info/, where data from [47] and [48] are presented.

The field enhancement near the surface of a NP can be described by the formula:

$$u = \gamma_E u(v_{if}), (2)$$

where u and u (v_{if}) are the energy of the external field in a unit spectral range with and without a nanoparticle, γ_E is the field enhancement factor equal to the ratio of the field generated by the particle to the initial one:

$$\gamma_E = \left|\frac{E}{E_0}\right|^2, (3)$$

where E is the field created by the particle, E_0 is the incident field.

The calculation made it possible to obtain the dependences of the absorption and scattering cross sections, as well as to calculate the field enhancement factor depending on the wavelength of the incident radiation in the medium containing the simulated NPs. Scattering by dimers consisting of two NPs with a radius of 10 and 30 nm located at a distance of 1, 5, 10, and 50 nm from each other was calculated using the finite difference time domain (FDTD) method [49, 50]. The finite difference method was used to numerically solve partial differential equations for three-dimensional

objects. In the calculation, it was assumed that the dimer is illuminated by a plane wave propagating along the z-axis and polarized along x-axis. The calculation takes into account the geometric parameters of the NPs and the dielectric constants of the medium and NPs. The calculation of the spatial distribution of the field and the local field enhancement between the particles was carried out for 458 and 561 nm wavelengths, which were used in the experiment.

Simulation of NP heating under the laser irradiation

Heating was calculated using the formula derived in [50]:

$$\Delta T_{NP} = \frac{\sigma_{abs} I}{4\pi R \kappa_{water}} = \frac{P}{4\pi R \kappa_{water}}, (4)$$

where σ_{abs} is the absorption cross section of the nanoparticle, I is the intensity of the incident laser radiation (W/m^2), P is the absorbed power (W), R is the nanoparticle radius, κ_{water} is the thermal conductivity of water, 0.56 W/(m·K). The heating was calculated using the absorption and scattering cross-sections calculated with the T-matrix method for the corresponding wavelengths.

Equation (4) makes it possible to calculate the heating of nanoparticles located in water irradiated with continuous laser radiation. The source of heat is optical absorption, which is locally proportional to the electric field strength and the imaginary part of the dielectric constant. We considered that water does not absorb the incident laser radiation. Thus, laser radiation is absorbed only by IONPs and creates a heating source located completely inside the nanoparticle. Due to the large difference in the thermal conductivity of water and Fe_2O_3 (0.56 and 7 W/(m·K) for water and iron oxide Fe_2O_3, respectively) we can assume that heat is distributed inside a particle so quickly, compared to the external environment, that its temperature is almost uniform for medium-sized particles, and thermal energy accumulates at the particle boundary before diffusing into the water. It should be noted that this approach was proposed by the authors of [51] for gold NPs in water, the difference in the thermal conductivity of gold and water is significantly higher (318 W/(m·K) for gold). However, in addition to the ratio of thermal conductivities, one should also take into account the time required to reach the steady state τ, which can be calculated as:

$$\tau \sim R^2 \frac{\rho c_p}{\kappa} = \frac{R^2}{9D}, (5)$$

where R is the radius of the nanoparticle, D is the thermal diffusivity (m^2/s). For water, the thermal diffusivity is 1.43×10^{-8} m^2/s.

The authors considered gold NPs 100 nm in size. The largest size of the NPs considered in this work is 70 nm. Due to the quadratic dependence of τ on the NP radius, the time to reach the steady state for our NPs is significantly shorter.

Since the temperature distribution corresponds to the Poisson equation, which is scale-invariant, it depends on the particle size only indirectly, through the absorbed power P. For a small sphere, the distribution $P(r)$ is uniform, and the temperature rise inside the NP can be described by the equation:

$$\Delta T(r) = \frac{p(R^2 - r^2)}{6\kappa_{NP}} + \Delta T_{NP}, (6)$$

where ΔT_{NP} is the temperature calculated using (4).

The temperature is the highest at the center of the particle, and tends to T_{NP} at the surface of the particle. Thermal heterogeneity can be calculated using the formula:

$$\frac{\Delta T_{max}}{\Delta T_{min}} = 1 + \frac{\kappa_{water}}{2\kappa_{NP}}, (7)$$

For Fe_2O_3 NPs, the ratio $\Delta T_{max}/\Delta T_{min}$ is 1.04. It can be said that the heat inside the NPs propagates rather quickly compared to the external environment, and the temperature is almost uniform inside the particles of the considered sizes. Thus, the approach proposed for gold nanoparticles is applicable to the IONPs considered in this work.

Results

The TEM results show that the IONPs of hexagonal shape and have diameters ranging from 20 to 70 nm (Fig. 1). The hydrodynamic size of particles in the colloid is 130±65 nm, which indicates some aggregation, the ζ-potential measured in distilled water (pH = 7.0) was 35±4 mV.

The intracellular distribution of IONPs in HeLa cell culture obtained using laser scanning microscopy is shown in Fig. 2.

In cells, "hot spots" are localized within endolysosomes, which is confirmed by the rapid discoloration of the lysosomal dye LysoTracker™ Green DND-26 (Invitrogen, USA), data not shown. A similar intracellular localization of IONPs is observed in many works, for example [32]. The emission spectra of "hot spots" are shown in Fig. 3.

The shape of the recorded spectra of "hot spots" is characteristic for thermal radiation, which indicates a high local temperature. To analyze and interpret the observed effect, we performed theoretical modeling of the local field enhancement between IONPs with a radius of 10 and 35 nm (the largest and smallest NP size

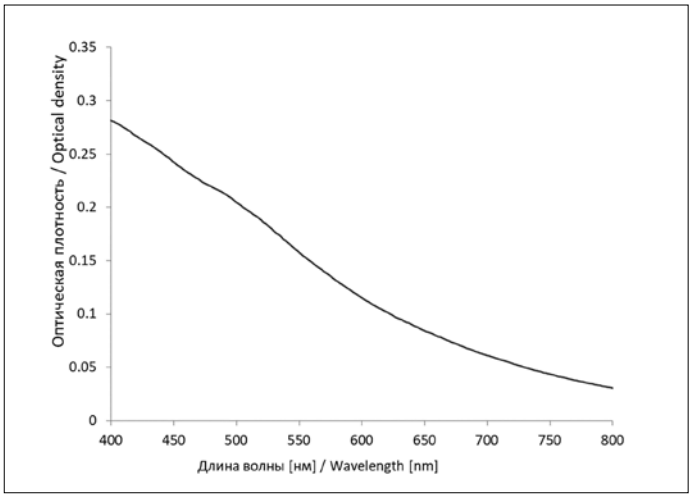

a

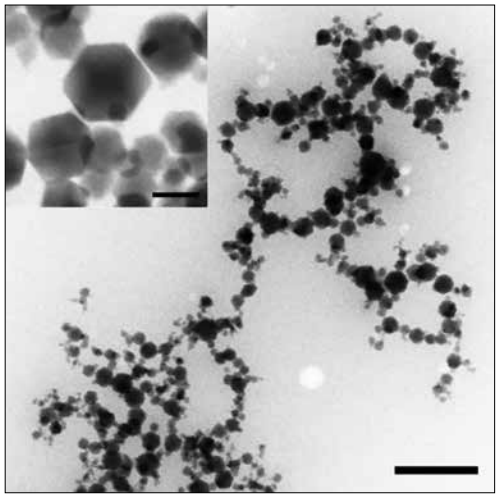

b

Рис. 1. a – спектры поглощения водного коллоида IONPs; b – ПЭМ IONPs, шкала 200 нм, на вставке – 30 нм.
Fig. 1. a – absorption spectra of IONPs water colloid; b – TEM of IONPs, scale 200 nm, scale on the inset – 30 nm.

in the studied colloids) and the heating of IONPs under the laser irradiation. The scattering and absorption cross-sections for single IONPs with a radius of 10 and 35 nm, calculated using the T-matrix method, are shown in Fig. 4.

The dependence of the field enhancement for single IONPs with a radius of 10 and 35 nm from the wavelength, calculated using the T-matrix method, is shown in Fig. 5.

It can be seen that the observed field enhancement for individual IONPs is rather low. For a pair of two particles, the field enhancement is much higher, Fig. 6.

The maximum enhancement is achieved at a small distance between nanoparticles and is 112 and 96 at a distance between nanoparticles of 1 nm for 458 and 561 nm wavelengths, respectively. These field enhancement values are comparable to the enhancement obtained with gold NPs. The field enhancement factor exponentially depends on the distance between particles, Fig. 5, and tends to the value for a large particle at large distances between particles. The calculated

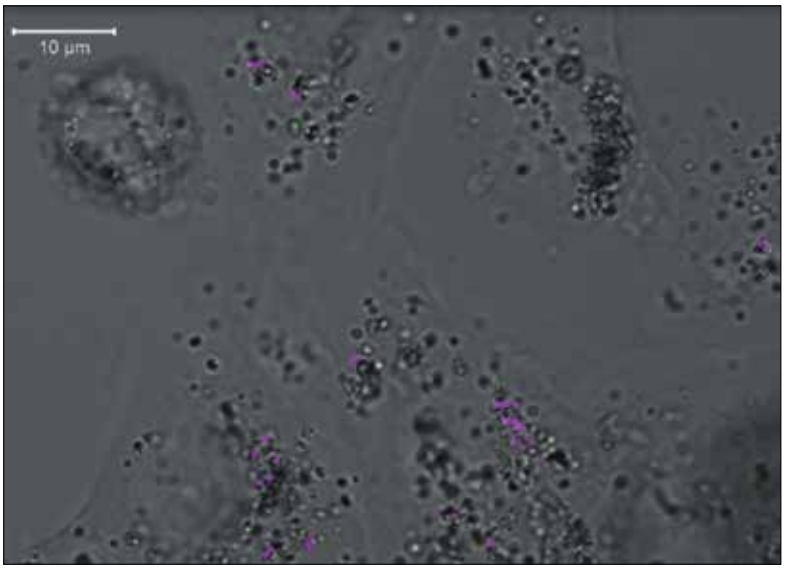

Рис. 2. Микроскопические изображения культуры клеток HeLa, полученные при лазерном сканировании с длиной волны 561 нм. Фиолетовым цветом показаны индуцируемые при лазерном сканировании «горячие точки».
Fig. 2. Microscopic images of a HeLa cell culture obtained by laser scanning at a wavelength of 561 nm. The «hot spots» induced by laser scanning are shown in purple.

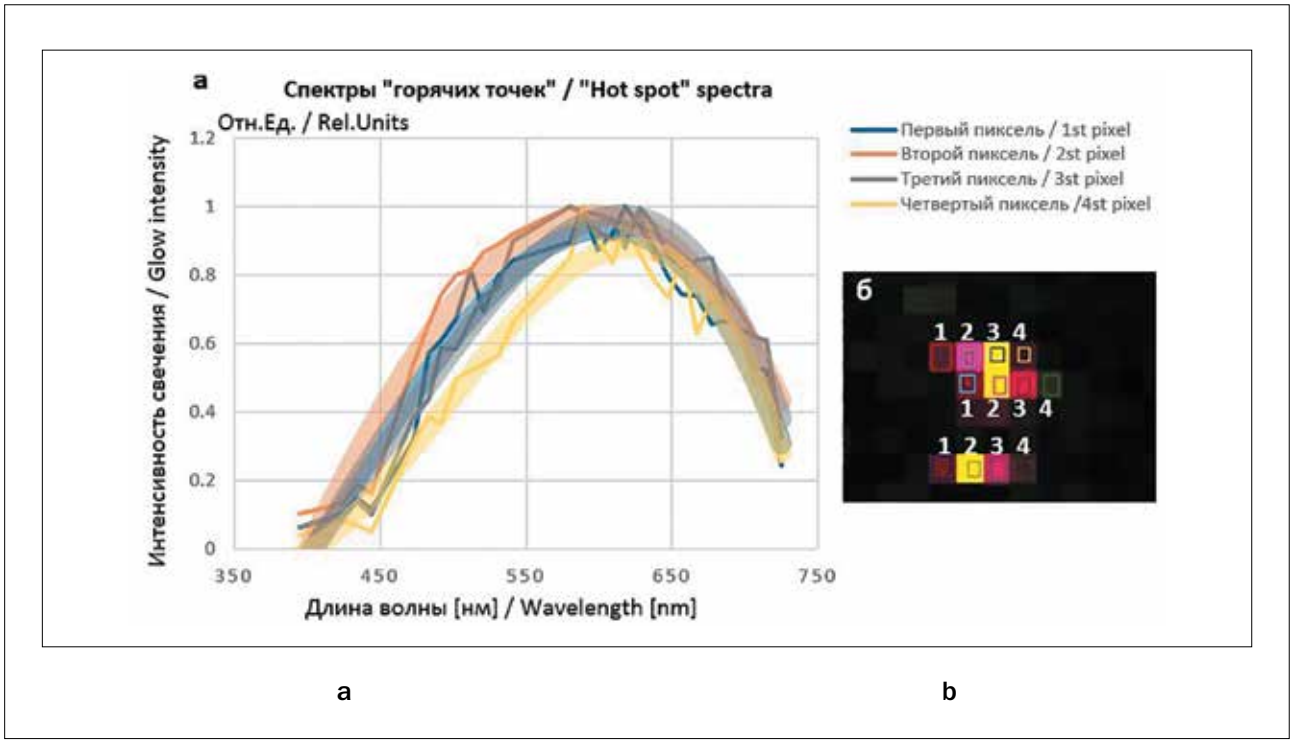

Рис. 3. a – спектры индуцируемых при лазерном сканировании «горячих точек», b – иллюстрация используемого метода усреднения. Показаны три «горячие точки», представляющие собой группу пикселей с различной яркостью. Для получения результирующих спектров проводили усреднение по пикселям с одинаковой яркостью (пиксель 1, пиксель 2 и т. д.) для четырех «горячих точек».
Fig. 3. a – spectra of laser-scanned «hot spots», b – illustration of the averaging method used. Three «hot spots» are shown, which are a group of pixels with different brightness. To obtain the resulting spectra, averaging was performed over pixels with the same brightness (pixel 1, pixel 2, etc.) for four «hot spots».

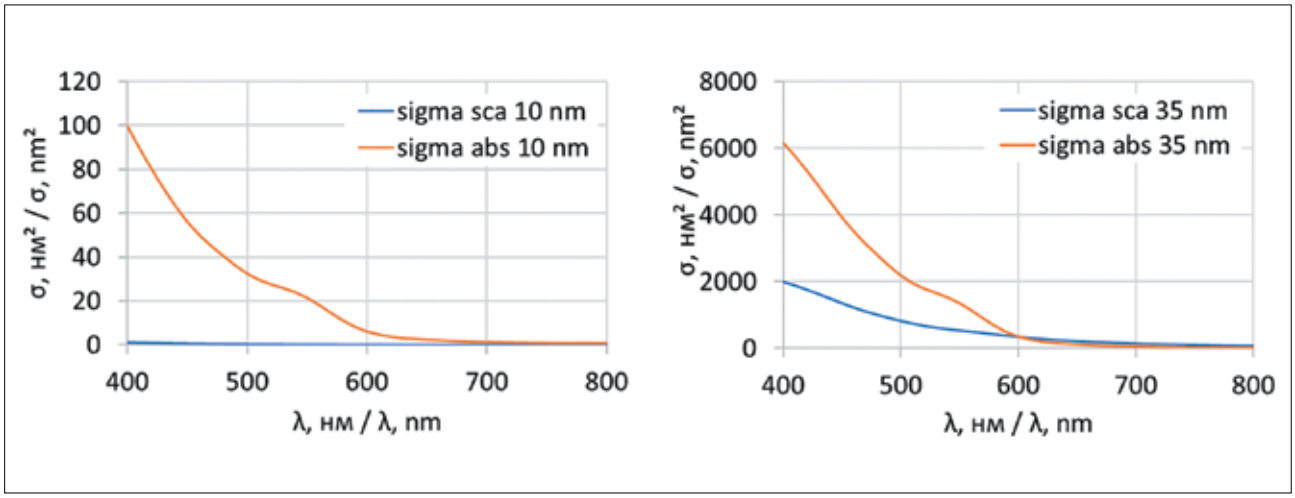

Рис. 4. Сечения рассеяния и поглощения для одиночных IONPs радиусом 10 нм и 35 нм, рассчитанные при помощи метода Т-матриц.
Fig. 4. Scattering and absorption cross sections for single IONPs with a radius of 10 nm and 35 nm, calculated using the T-matrix method.

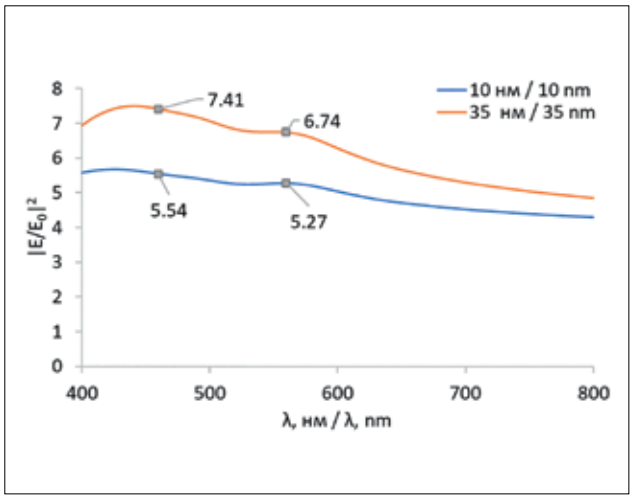

Рис. 5. Фактор усиления поля для одиночных IONPs радиусом 10 нм и 35 нм, рассчитанный при помощи метода Т-матриц. Сносками показаны значения фактора усиления поля для длин волн 458 нм и 561 нм.
Fig. 5. Field enhancement factor for single IONPs with a radius of 10 nmand 35 nm, calculated using the T-matrix method. Data labels show the values of the field amplification factor for the wavelengths of 458 nm and 561 nm.

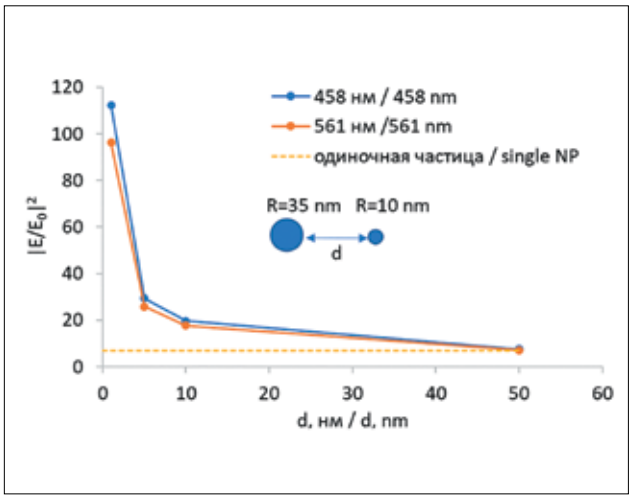

Рис. 6. Фактор усиления поля для димеров из двух IONPs радиусами 10 нм и 35 нм, рассчитанный при помощи метода конечных разностей во временной области для длин волн 458 нм и 561 нм в зависимости от расстояния между наночастицами *d*.
Fig. 6. Field enhancement factor for dimers from IONPs with a radius of 10 nm and 35 nm, calculated using the finite difference method in the time domain for wavelengths of 458 nm and 561 nm depending on the distance between nanoparticles *d*.

enhancement values for single IONPs and dimers are shown in Table 1.

When analyzing the results obtained for the spatial distribution of the field, several characteristic zones can be distinguished in the EM interaction of two particles, Fig. 7.

At distances of more than 10 nm, the particles practically do not interact with each other. The enhancement is almost the same as for individual IONPs (Table 1). As the distance decreases to less than 10 nm, the field enhancement zones around the nanoparticles begin to overlap and local "hot spots" appear, the enhancement in which significantly exceeds the field enhancement for individual NPs. With a change in the distance from 10 to 1 nm, an exponential increase in the field enhancement factor is observed, as well as localization of the resulting enhancement in a small region of the space between NPs.

The values of the heating temperature under the laser irradiation, calculated for IONPs with a radius of 10 and 35 nm (the smallest and largest particle size in a colloid), under the laser irradiation with wavelengths of 458 and 561 nm, are shown in Table 2.

It is shown that the heating temperature of large NPs (70 nm in size) approximately corresponds to the heating temperature of 100 nm gold NPs by laser radiation at the absorption maximum. The total heating of a 100 nm NP by two wavelengths is 107.9 °C. Despite the rather high heating temperature, the occurrence of thermal emission of nanoparticles at

Таблица 1
Фактор усиления поля, рассчитанный для одиночных IONP и их димеров
Table 1
Field enhancement factor calculated for single IONPs and their dimers

Димеры IONPs IONPs dimers		
Параметр Parameter	$\|E/E_0\|^2$	$\|E/E_0\|^2$
d, нм d, nm	λ = 458 нм λ = 458 nm	λ = 561 нм λ = 561 nm
1	112	96
5	29	26
10	20	18
50	8	7
Одиночные IONPs Single IONPs		
	$\|E/E_0\|^2$	$\|E/E_0\|^2$
λ, нм λ, nm	R = 10 нм R = 10 nm	R = 35 нм R = 35 nm
460	6	8
560	5	7

Примечание: *d* – расстояние между наночастицами, λ – длина волны, R – радиус наночастиц.
Note: d – distance between nanoparticles, λ – wavelength, R – radius of nanoparticles.

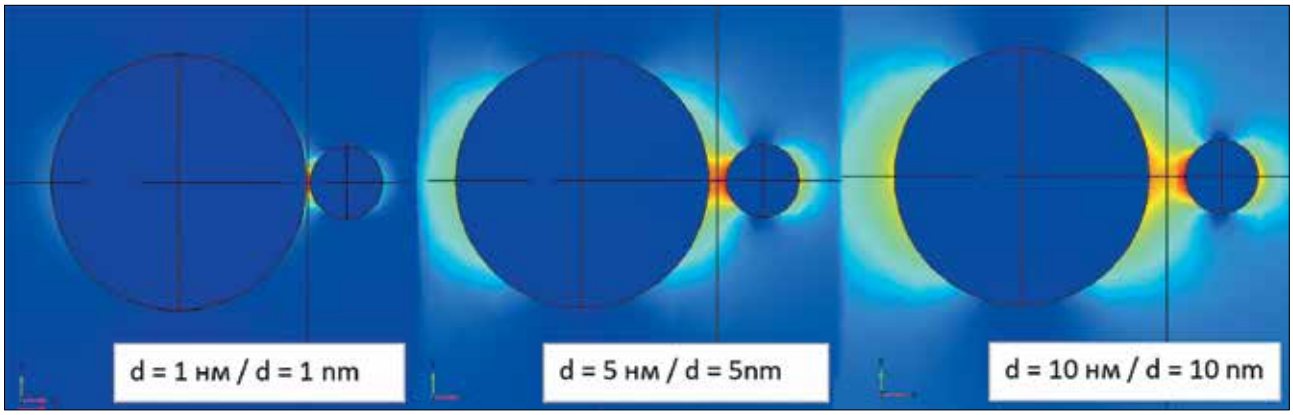

Рис. 7. Пространственное распределение поля и локального усиления поля между IONPs с радиусами 10 нм и 35 нм в зависимости от расстояния между наночастицами *d*.
Fig. 7. Spatial field distribution and local field enhancement between IONPs with 10 nm and 35 nm radii depending on distance between NPs *d*.

Таблица 2
Время достижения установившегося режима τ и относительное изменение температуры ΔT под действием лазерного излучения для исследованных IONPs
Table 2
Time to reach steady state conditions τ and relative temperature change ΔT under the laser irradiation for the studied IONPs

НЧ / NPs	Среда / Medium	R, нм / R, nm	τ, мкс / τ, μs	σ_{abs}, нм^2 / σ_{abs}, nm^2	ΔT, °C	Источник / Reference
Fe_2O_3	вода	10	0.001	50 (458 нм) 18 (560 нм)	4.4 1.1	эта работа / this work
Fe_2O_3		35	0.003	3522 (458 нм) 1157 (560 нм)	88.9 19.0	эта работа / this work
Au		50	0.019	(в работе не указано) / NA	100	[50]

Примечание: R – радиус наночастиц, τ – время достижения установившегося режима, σ_{abs} – сечение поглощения наночастицы, ΔT – относительное изменение температуры под действием лазерного излучения.
Note: R – radius of nanoparticles, τ – time to reach steady state conditions, σ_{abs} – absorption cross section of nanoparticle, ΔT – relative temperature change under the laser irradiation.

such temperatures is unlikely. In this regard, we assume that the observed "hot spots" arise mainly due to the local field enhancement.

Since the field enhancement is highly dependent on the distance between particles, we investigated the effect of temperature on the number of observed "hot spots". Presumably, as the temperature rises, the particles more often find themselves at a close distance from each other and the number of observed "hot spots" should increase.

The IONPs colloid image obtained by laser scanning at wavelengths of 488 and 561 nm is shown in Fig. 8a. The dependence of the number of "hot spots" on temperature and particle concentration is shown in Fig. 8b.

With an increase in temperature by 30°C, the number of "hot spots" increased by about 7000 on average. This is

due to the fact that with an increase in temperature, the diffusion coefficient increases, which is proportional to the temperature, and the particles more often approach each other. Thus, due to more frequent approaches of nanoparticles, enhancement occurs more often, which confirms the assumption made about the appearance of the observed "hot spots" due to the local enhancement of the electromagnetic field between NPs.

Discussion and conclusion

Over the past 20 years, there has been a significant increase in the number of reports on hyperthermia. Many focused on the local heating effect, a special temperature profile near NPs with little or no macroscopic heating. This approach has many benefits. First, the effect becomes less dependent on the number of NPs usually required to significantly increase the macroscopic temperature in the target area. Consequently, biological tissues are not exposed to serious stress, and the toxic effects are highly localized. Second, the thermal profile around the NP can cause drug release without thermal damage to the treatment area.

The temperature profile of heating near a nanoparticle is difficult to study due to its nanoscopic size and short event time. Measurements can be an indirect (for example, using thermosensitive reactions) or a direct estimate of the thermal gradient in the region of interest. Direct estimation of the local temperature profile around nanoparticles is less studied [52]. Using nanotherometers, such as up-conversion NPs [53], sensors based on DNA hybridization [54], thermosensitive polymers [55], a strong temperature gradient was recorded from the surface of nanoparticles to the environment.

Another interesting effect is the local enhancement of the electromagnetic field near nanoparticles, which can lead to an increase in the luminescence intensity of nanoparticles and dyes [56], an increase in the Raman scattering signal [57], and an increase in the efficiency of singlet oxygen generation by photosensitizers [58]. It was shown in [59] that the field enhancement for non-spherical gold nanoparticles E/E_0 is 25 to 35 times. The use of dimers made of non-spherical gold nanoparticles and careful optimization of their parameters made it possible to obtain a field enhancement of 270 for two gold nanoparticles, elliptical and spherical, differing 1000 times in volume, located at a distance of 17 nm from each other. The field enhancement between two spherical silver nanoparticles with a radius of 0.5 and 5 nm exceeds the field enhancement of one NP by a factor of 75 and is about 400 at the resonance wavelength.

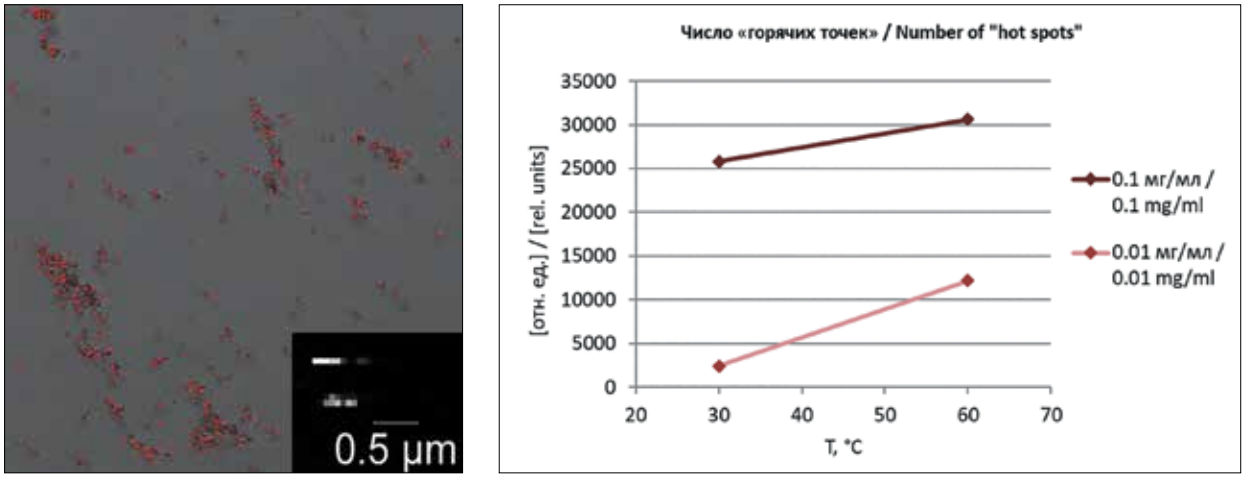

a b

Рис. 8. a – красным цветом представлены «горячие точки» для водного коллоида IONPs с концентрацией 0,1 мг/мл при облучении одновременно лазерами с длинами волн 488 нм и 561 нм при 100% мощности; b – зависимости количества наблюдаемых вспышек от концентрации IONPs и температуры.

Fig. 8. a – red color represents «hot spots» for an aqueous colloid of IONPs with a concentration of 0.1 mg/ml under simultaneous irradiation with 488 nm and 561 nm lasers at 100% power; b – dependences of the number of observed «hot spots» on the concentration of IONPs and temperature.

In our work, we have demonstrated that, upon laser excitation of the investigated IONPs, individual regions with a bright glow, the so-called "hot spots", are observed in the obtained images. In the case of *in vitro* studies, these points were localized in areas of accumulation of nanoparticles inside cells, presumably in lysosomes. Exposure of cell cultures to high power density laser radiation leads to cell death. It was assumed that the cause of the observed effect may be laser-induced heating and / or local enhancement of the electromagnetic field near the surface of nanoparticles.

Based on our recorded luminescence spectra of "hot spots" in an aqueous colloid of polydisperse IONPs at a sufficiently high laser scanning power density (MW/cm^2) characteristic of thermal radiation, conclusions can be drawn about a very high local temperature.

However, using theoretical modeling, it was shown that the heating temperature of large NPs (70 nm in size) approximately corresponds to the heating temperature of 100 nm gold NPs by continuous laser radiation to the absorption maximum. The total heating of a 100 nm NP by two wavelengths is 107.9 °C. Despite the rather high heating temperature, the occurrence of thermal emission of nanoparticles at such temperatures is unlikely. However, upon reaching 100 °C, water begins to boil, the NP will end up in a vapor bubble, this will reduce the rate of heat dissipation and lead to even greater overheating. It should be noted that, according to the literature data, in the case of pulsed laser excitation, heating can be significantly higher and reach 1000 K at the end of the laser pulse [60].

Theoretical modeling of the local field enhancement for IONPs with a radius of 10 and 35 nm showed that the dependence of the enhancement for single NPs is rather low. For a pair of particles with a radius of 10 and 35 nm, the field enhancement is much higher. The maximum enhancement is achieved at a small distance between nanoparticles and is two orders of magnitude at a distance between nanoparticles of 1 nm. Such values of the field enhancement are comparable to the enhancement obtained for plasmonic NPs made of noble metals.

At distances more than 10 nm, the particles practically do not interact with each other. When the distance changes from 10 to 1 nm, an exponential increase in the field enhancement factor is observed, as well as localization of the resulting enhancement in a small region of the space between nanoparticles, and local "hot spots" appear. It was also shown in [60] that, in contrast to single spherical nanoparticles, for which a uniform temperature distribution is observed in the bulk of the nanoparticle, in the case of dimers and trimers from gold nanoparticles, hot and cold zones arise in the bulk of the particles with plasmon resonance. The location of the maximum density of the plasma of free electrons surrounding the nanoparticles coincides with the location of the "hot spots" of the hot zones with high temperature and with the location of the maximum enhancement of the electric field inside the particles. Thus, the observed thermal emission may be due to the local enhancement of the electric field in IONPs dimers.

Funding
This work was funded by the RFBR, grant 21-52-12030.

REFERENCES

1. X. Xu, W. Ho, X. Zhang, N. Bertrand, and O. Farokhzad, Cancer nanomedicine: from targeted delivery to combination therapy, *Trends in Molecular Medicine*, 2015, vol. 21, no. 4, pp. 223–232.
2. R. Borlan, M. Focsan, D. Maniu, and S. Astilean, Interventional NIR Fluorescence Imaging of Cancer: Review on Next Generation of Dye-Loaded Protein-Based Nanoparticles for Real-Time Feedback During Cancer Surgery, *IJN 16*, 2021, pp. 2147–2171.
3. B. S. Dash, S. Das, and J.-P. Chen, Photosensitizer-Functionalized Nanocomposites for Light-Activated Cancer Theranostics, *IJMS*, 2021, vol. 22, no. 13, pp. 6658.
4. G. Liu, L. Yang, G. Chen et al., A Review on Drug Delivery System for Tumor Therapy, *Front. Pharmacol*, 2021, vol. 12, pp. 735446
5. P. Wust, B. Hildebrandt, G. Sreenivasa, B. Rau, et al., Hyperthermia in combined treatment of cancer, *The Lancet Oncology*, 2002, vol. 3, no. 8, pp. 487–497.
6. J. Kolosnjaj-Tabi and C. Wilhelm, Magnetic nanoparticles in cancer therapy: how can thermal approaches help? *Nanomedicine*, 2017, vol. 12, no. 6, pp. 573–575.
7. Sidorov D.V., Grishin N.A., Lozhkin M.V., Troitsky A.A., Moshurov R.I., Bykasov S.A., Urlova A.N., Filonenko E.V. Intraoperative photodynamic therapy and hyperthermic intraperitoneal chemotherapy in cytoreductive treatment of patients with disseminated mucinous carcinoma of appendix, *Biomedical Photonics*, 2020, vol. 9, no. 4, pp. 23–30 (in Russian) doi: 10.24931/2413–9432–2020–9–4-23–30
8. Kaprin A.D., Mardinskiy Yu.S., Smirnov V.P., Ivanov S.A., Kostin A.A., Polikhov S.A., Reshetov I.V., Fatianova A.S., Denisenko M.V., Epatova T.V., Korenev S.V., Tereshchenko A.V., Filonenko E.V., Gafarov M.M., Romanko Yu.S. The history of radiation therapy (part I), *Biomedical Photonics*, 2019, vol. 8, no. 1, pp. 52–62 (in Russian). doi: 10.24931/2413–9432–2019–8–1–52–62
9. M.R. Horsman, Tissue physiology and the response to heat, *International Journal of Hyperthermia*, 2006, vol. 22, no. 3, pp. 197–203.
10. J. Kolosnjaj-Tabi, R. Di Corato, L. Lartigue, et al., Heat-Generating Iron Oxide Nanocubes: Subtle "Destructurators" of the Tumoral Microenvironment, *ACS Nano*, 2014, vol. 8, no. 5, pp. 4268–4283.
11. F. Mohamed, P. Marchettini, O.A. Stuart et al., Thermal Enhancement of New Chemotherapeutic Agents at Moderate Hyperthermia, *Ann Surg Oncol*, 2003, vol. 10, no. 4, pp. 463–468.
12. R. Issels, Hyperthermia Combined with Chemotherapy – Biological Rationale, Clinical Application, and Treatment Results, *Oncol Res Treat*, 1999, vol. 22, no. 5, pp. 374–381.
13. H.D. Suit and L.E. Gerweck, Potential for hyperthermia and radiation therapy, *Cancer Res*, 1979, vol. 39 (6 Pt 2), pp. 2290–2298.
14. S. Spirou, M. Basini, A. Lascialfari et al., Magnetic Hyperthermia and Radiation Therapy: Radiobiological Principles and Current Practice, *Nanomaterials*, 2018, vol. 8, no. 6, pp. 401.
15. O. Dahl, Status of Clinical Hyperthermia, *Acta Oncologica*, 1999, vol. 38, no. 7, pp. 863–873.
16. K. Hynynen, D. Shimm, D. Anhalt et al., Temperature distributions during clinical scanned, focused ultrasound hyperthermia treatments, *International Journal of Hyperthermia*, 1990, vol. 5, no. 5, pp. 891–908.
17. Gorshkova A.S., Shilov I.P., Ivanov A.V., Rumyantseva V.D. Synthesis and research of nanoparticles for magnetic-luminescent tumor theranostics based on the Yb-complex of DME protoporphyrin IX and iron oxide. Proceedings of the IX International Congress "Photodynamic therapy and photodiagnostics" Moscow October 23–24, 2020, *Biomedical Photonics*. 2020, vol. 8, no. 4s, pp. 5–6.
18. V. Mulens-Arias, J.M. Rojas, and D.F. Barber, The Use of Iron Oxide Nanoparticles to Reprogram Macrophage Responses and the Immunological Tumor Microenvironment. *Front. Immunol*, 2021, vol. 12, pp. 693709.

ЛИТЕРАТУРА

1. Xu X., Ho W., Zhang X., Bertrand N. and Farokhzad O. Cancer nanomedicine: from targeted delivery to combination therapy//Trends in Molecular Medicine. – 2015. –Vol. 21 (4). – P. 223–232.
2. Borlan R., Focsan M., Maniu D. and Astilean S. Interventional NIR Fluorescence Imaging of Cancer: Review on Next Generation of Dye-Loaded Protein-Based Nanoparticles for Real-Time Feedback During Cancer Surgery//IJN 16. – 2021. – P. 2147–2171.
3. Dash B.S., Das S., Chen J.-P. Photosensitizer-Functionalized Nanocomposites for Light-Activated Cancer Theranostics//IJMS. 2021. – 22 (13). – P. 6658.
4. Liu G., Yang L., Chen G. et al. A Review on Drug Delivery System for Tumor Therapy//Front. Pharmacol. – 2021. – Vol.12. – P. 735446
5. Wust P., Hildebrandt B., Sreenivasa G., Rau B. et al. Hyperthermia in combined treatment of cancer//The Lancet Oncology. – 2002. – Vol. 3 (8). – P. 487–497.
6. Kolosnjaj-Tabi J., Wilhelm C. Magnetic nanoparticles in cancer therapy: how can thermal approaches help?//Nanomedicine. – 2017. – Vol. 12 (6). – P. 573–575.
7. Сидоров Д.В., Гришин Н.А., Ложкин М.В., Троицкий А.А., Мошуров Р.И., Быкасов С.А., Урлова А.Н., Филоненко Е.В. Интраоперационная фотодинамическая терапия и гипертермическая внутрибрюшная химиотерапия при циторедуктивном хирургическом лечении больных диссеминированной муцинозной карциномой аппендикса//Biomedical Photonics. 20. – Т. 9, № 4. – P. 23–30. https://doi.org/10.24931/2413–9432–2020–9-4–23–30
8. Каприн А.Д., Мардынский Ю.С., Смирнов В.П., Иванов С.А., Костин А.А., Полихов С.А., Решетов И.В., Фатьянова А.С., Денисенко М.В., Эпатова Т.В., Коренев С.В., Терещенко А.В., Филоненко Е.В., Гафаров М.М., Романко Ю.С. К истории развития лучевой терапии (часть I)//Biomedical Photonics. – 2019. – Т. 8, № 1. – С. 52–62. doi: 10.24931/2413–9432–2019–8–1–52–62.
9. Horsman M.R. Tissue physiology and the response to heat//International Journal of Hyperthermia. – 2006. – Vol. 22 (3). – P. 197–203.
10. Kolosnjaj-Tabi J., Di Corato R., Lartigue L. et al. Heat-Generating Iron Oxide Nanocubes: Subtle "Destructurators" of the Tumoral Microenvironment//ACS Nano. –2014. – Vol. 8 (5). – P. 4268–4283.
11. Mohamed F., Marchettini P., Stuart O.A. et al. Thermal Enhancement of New Chemotherapeutic Agents at Moderate Hyperthermia//Ann Surg Oncol. – 2003. – Vol. 10 (4). – P. 463–468.
12. Issels R. Hyperthermia Combined with Chemotherapy – Biological Rationale, Clinical Application, and Treatment Results//Oncol Res Treat. – 1999. – Vol. 22 (5). – P. 374–381.
13. Suit H.D. and Gerweck L.E., Potential for hyperthermia and radiation therapy//Cancer Res. – 1979. – Vol. 39 (6 Pt 2). – P. 2290–2298.
14. Spirou S., Basini M., Lascialfari A. et al. Magnetic Hyperthermia and Radiation Therapy: Radiobiological Principles and Current Practice//Nanomaterials. – 2018. –Vol. 8 (6). – P. 401.
15. Dahl O. Status of Clinical Hyperthermia//Acta Oncologica. – 1999. – Vol. 38 (7). – P. 863–873.
16. Hynynen K., Shimm D., Anhalt D. et al. Temperature distributions during clinical scanned, focused ultrasound hyperthermia treatments//International Journal of Hyperthermia. – 1990. – Vol. 6 (5). – P. 891–908.
17. Горшкова А.С., Шилов И.П., Иванов А.В., Румянцева В.Д. Синтез и исследование наночастиц для магнитно-люминесцентеной тераностики опухолей на основе Yb-комплекса ДМЭ протопорфирина IX и оксида железа//Материалы IX Международного конгресса «Фотодинамическая терапия и фотодиагностика» Москва 23–24 октября 2020 г. Biomedical Photonics. 20. – Т. 9, № 4s. – P. 5–6.

19. S. Zanganeh, G. Hutter, R. Spitler et al., Iron oxide nanoparticles inhibit tumour growth by inducing pro-inflammatory macrophage polarization in tumour tissues. *Nature Nanotech*, 2016, vol. 11, no. 11, pp. 986–994.
20. U. S. Gaharwar, R. Meena, and P. Rajamani, Iron oxide nanoparticles induced cytotoxicity, oxidative stress and DNA damage in lymphocytes: Iron oxide nanoparticles toxicity in lymphocytes, *J. Appl. Toxicol*, 2017, vol. 37, no. 10, pp. 1232–1244.
21. M. A. Malvindi, V. De Matteis, A. Galeone et al., Toxicity Assessment of Silica Coated Iron Oxide Nanoparticles and Biocompatibility Improvement by Surface Engineering, *PLoS ONE*, 2014, Vol. 9 (1), pp. e85835.
22. L. Arias, J. Pessan, A. Vieira et al., Iron Oxide Nanoparticles for Biomedical Applications: A Perspective on Synthesis, Drugs, Antimicrobial Activity, and Toxicity, *Antibiotics*, 2018, vol. 7, no. 2, pp. 46.
23. R. Sun, H. Chen, L. Sutrisno, N. Kawazoe, and G. Chen, Nanomaterials and their composite scaffolds for photothermal therapy and tissue engineering applications, Science and *Technology of Advanced Materials*, 2021, vol. 22, no. 1, pp. 404–428.
24. Q. Liu, L. Liu, C. Mo, X. Zhou et al., Polyethylene glycol-coated ultrasmall superparamagnetic iron oxide nanoparticles-coupled sialyl Lewis X nanotheranostic platform for nasopharyngeal carcinoma imaging and photothermal therapy, J Nanobiotechnol, 2021, vol. 19, no. 1, pp. 171.
25. J. G. Ovejero, I. Armenia, D. Serantes et al., Selective Magnetic Nanoheating: Combining Iron Oxide Nanoparticles for Multi-Hot-Spot Induction and Sequential Regulation, *Nano Lett*, 2021, vol. 21, no. 17, pp. 7213–7220.
26. D. Shi, M. E. Sadat, A. W. Dunn, and D. B. Mast, Photo-fluorescent and magnetic properties of iron oxide nanoparticles for biomedical applications, *Nanoscale*, 2015, vol. 7, no. 18, pp. 8209–8232.
27. G. Vallejo-Fernandez, O. Whear, A. G. Roca et al., Mechanisms of hyperthermia in magnetic nanoparticles, *J. Phys. D: Appl. Phys*, 2013, vol. 46, no. 31, pp. 312001.
28. A. Espinosa, J. Kolosnjaj-Tabi, A. Abou-Hassan et al., Magnetic (Hyper)Thermia or Photothermia? Progressive Comparison of Iron Oxide and Gold Nanoparticles Heating in Water, in Cells, and In Vivo, *Adv. Funct. Mater*, 2018, vol. 28, no. 37, pp. 1803660.
29. M. Johannsen, U. Gneveckow, B. Thiesen et al., Thermotherapy of Prostate Cancer Using Magnetic Nanoparticles: Feasibility, Imaging, and Three-Dimensional Temperature Distribution, *European Urology*, 2007, vol. 52, no. 6, pp. 1653–1662.
30. P. Guardia, R. Di Corato, L. Lartigue et al., Water-Soluble Iron Oxide Nanocubes with High Values of Specific Absorption Rate for Cancer Cell Hyperthermia Treatment, *ACS Nano*, 2012, vol. 6, no. 4, pp. 3080–3091.
31. C. Martinez-Boubeta, K. Simeonidis, A. Makridis et al., Learning from Nature to Improve the Heat Generation of Iron-Oxide Nanoparticles for Magnetic Hyperthermia Applications, *Sci Rep*, 2013, vol. 3, no. 1, pp. 1652.
32. A. Espinosa, R. Di Corato, J. Kolosnjaj-Tabi et al., Duality of Iron Oxide Nanoparticles in Cancer Therapy: Amplification of Heating Efficiency by Magnetic Hyperthermia and Photothermal Bimodal Treatment, *ACS Nano*, 2016, vol. 10, no. 2, pp. 2436–2446.
33. H. Yan, W. Shang, X. Sun, L. Zhao et al., "All-in-One" Nanoparticles for Trimodality Imaging-Guided Intracellular Photo-magnetic Hyperthermia Therapy under Intravenous Administration, *Adv. Funct. Mater*, 2018, vol. 28, no. 9 pp. 1705710.
34. S.-Y. Lin, R.-Y. Huang, W.-C. Liao et al., Multifunctional PEGylated Albumin/IR780/Iron Oxide Nanocomplexes for Cancer Photothermal Therapy and MR Imaging, *Nanotheranostics*, 2018, vol. 2, no. 2, pp. 106–116.
35. S. Cabana, A. Curcio, A. Michel, C. Wilhelm, and A. Abou-Hassan, Iron Oxide Mediated Photothermal Therapy in the Second Biological Window: A Comparative Study between Magnetite/Maghemite Nanospheres and Nanoflowers, *Nanomaterials*, 2020, vol. 10, no. 8, pp.1548.

18. Mulens-Arias V., Rojas J. M. and Barber D. F. The Use of Iron Oxide Nanoparticles to Reprogram Macrophage Responses and the Immunological Tumor Microenvironment//Front. Immunol. – 2021. – Vol. 12. – P. 693709.
19. Zanganeh S., Hutter G., Spitler R. et al. Iron oxide nanoparticles inhibit tumour growth by inducing pro-inflammatory macrophage polarization in tumour tissues//Nature Nanotech. – 2016. – Vol. 11 (11). – P. 986–994.
20. Gaharwar U. S. Meena R., and Rajamani P., Iron oxide nanoparticles induced cytotoxicity, oxidative stress and DNA damage in lymphocytes: Iron oxide nanoparticles toxicity in lymphocytes//J. Appl. Toxicol. – 2017. – Vol. 37 (10). – P. 1232–1244.
21. Malvindi M. A., Matteis V. De, A Galeone. et al. Toxicity Assessment of Silica Coated Iron Oxide Nanoparticles and Biocompatibility Improvement by Surface Engineering//PLoS ONE. – 2014. – Vol. **9** (1). – P. e85835.
22. Arias L., Pessan J., Vieira A. et al. Iron Oxide Nanoparticles for Biomedical Applications: A Perspective on Synthesis, Drugs, Antimicrobial Activity, and Toxicity//Antibiotics. – 2018. – Vol. 7 (2). – P. 46.
23. Sun R., Chen H., Sutrisno L., Kawazoe N., and Chen G., Nanomaterials and their composite scaffolds for photothermal therapy and tissue engineering applications//Science and Technology of Advanced Materials. – 2021. – Vol. 22 (1). – P. 404–428.
24. Liu Q., Liu L., Mo C., Zhou X. et al. Polyethylene glycol-coated ultrasmall superparamagnetic iron oxide nanoparticles-coupled sialyl Lewis X nanotheranostic platform for nasopharyngeal carcinoma imaging and photothermal therapy//J Nanobiotechnol. – 2021. – Vol. 19 (1). – P. 171.
25. Ovejero J. G., Armenia I., Serantes D. et al. Selective Magnetic Nanoheating: Combining Iron Oxide Nanoparticles for Multi-Hot-Spot Induction and Sequential Regulation//Nano Lett. – 2021. – Vol. 21 (17). – P. 7213–7220.
26. Shi D., Sadat M. E., Dunn A. W., and Mast D. B., Photo-fluorescent and magnetic properties of iron oxide nanoparticles for biomedical applications//Nanoscale. – 2015. – Vol. **7** (18). – P. 8209–8232.
27. Vallejo-Fernandez G., Whear O., Roca A. G. et al. Mechanisms of hyperthermia in magnetic nanoparticles//J. Phys. D: Appl. Phys. – 2013. – Vol. 46 (31). – P. 312001.
28. Espinosa A., Kolosnjaj-Tabi J., Abou-Hassan A. et al. Magnetic (Hyper)Thermia or Photothermia? Progressive Comparison of Iron Oxide and Gold Nanoparticles Heating in Water, in Cells, and In Vivo//Adv. Funct. Mater. – 2018. – Vol. 28 (37). – P. 1803660.
29. Johannsen M., Gneveckow U., Thiesen B. et al. Thermotherapy of Prostate Cancer Using Magnetic Nanoparticles: Feasibility, Imaging, and Three-Dimensional Temperature Distribution//European Urology. – 2007. – Vol. 52 (6). – P. 1653–1662.
30. Guardia P., R. Corato Di, Lartigue L. et al., Water-Soluble Iron Oxide Nanocubes with High Values of Specific Absorption Rate for Cancer Cell Hyperthermia Treatment//ACS Nano. – 2012. – Vol. 6 (4). – P. 3080–3091.
31. Martinez-Boubeta C., Simeonidis K., Makridis A. et al., Learning from Nature to Improve the Heat Generation of Iron-Oxide Nanoparticles for Magnetic Hyperthermia Applications//Sci Rep. – 2013. – Vol. 3 (1). – P. 1652.
32. Espinosa A., R. Corato Di, Kolosnjaj-Tabi J. et al., Duality of Iron Oxide Nanoparticles in Cancer Therapy: Amplification of Heating Efficiency by Magnetic Hyperthermia and Photothermal Bimodal Treatment//ACS Nano. –2016. – Vol. 10 (2). – P. 2436–2446.
33. Yan H., Shang W., X. Sun, L. Zhao et al., "All-in-One" Nanoparticles for Trimodality Imaging-Guided Intracellular Photo-magnetic Hyperthermia Therapy under Intravenous Administration//Adv. Funct. Mater. – 2018. – Vol. 28 (9). – P. 1705710.
34. Lin S.-Y., Huang R.-Y., Liao W.-C. et al. Multifunctional PEGylated Albumin/IR780/Iron Oxide Nanocomplexes for Cancer

36. J. Shi, X. Yu, L. Wang, Y. Liu et al., PEGylated fullerene/iron oxide nanocomposites for photodynamic therapy, targeted drug delivery and MR imaging, *Biomaterials*, 2013, vol. 34, no. 37, pp. 9666–9677.
37. O. Penon, M. J. Marín, D. B. Amabilino, D. A. Russell, and L. Pérez-García, Iron oxide nanoparticles functionalized with novel hydrophobic and hydrophilic porphyrins as potential agents for photodynamic therapy, *Journal of Colloid and Interface Science*, 2016, vol. 462, pp. 154–165.
38. V. V. Klimov, Nanoplasmonics. *2nd ed. Fizmatlit*, 2010.
39. M. V. Bashevoy, V. A. Fedotov, and N. I. Zheludev, Optical whirlpool on an absorbing metallic nanoparticle, *Opt. Express*, 2005, vol. 13, no. 21, pp. 8372.
40. S. K. Sharma, N. Shrivastava, F. Rossi et al., Nanoparticles-based magnetic and photo induced hyperthermia for cancer treatment, *Nano Today*, 2019, vol. 29, pp. 100795.
41. C. Lozano-Pedraza, E. Plaza-Mayoral, A. Espinosa, B. Sot, et al., Assessing the parameters modulating optical losses of iron oxide nanoparticles under near infrared irradiation, *Nanoscale Adv*, 2021, vol. 3, no. 22, pp. 6490–6502.
42. Y. Jeong, Y.-M. Kook, K. Lee, and W.-G. Koh, Metal enhanced fluorescence (MEF) for biosensors: General approaches and a review of recent developments, *Biosensors and Bioelectronics*, 2018, vol. 111, pp. 102–116.
43. M. M. Sigalas, D. A. Fattal, R. S. Williams, et al., Electric field enhancement between two Si microdisks, *Opt. Express*, 2007, vol. 15, no. 22, pp. 14711.
44. S. Toroghi and P. G. Kik, Photothermal response enhancement in heterogeneous plasmon-resonant nanoparticle trimmers, *Phys. Rev. B.*, 2014, vol. 90, no. 20, pp. 205414.
45. N. G. Khlebtsov, T-matrix method in plasmonics: An overview, *Journal of Quantitative Spectroscopy and Radiative Transfer*, 2013, vol. 123, pp. 184–217.
46. D. W. Mackowski and M. I. Mishchenko, A multiple sphere T-matrix Fortran code for use on parallel computer clusters, *Journal of Quantitative Spectroscopy and Radiative Transfer*, 2011, vol. 112, no. 13, pp. 2182–2192.
47. A. D. Rakić, A. B. Djurišić, J. M. Elazar, and M. L. Majewski, "Optical properties of metallic films for vertical-cavity optoelectronic devices, *Appl. Opt*, 1998, vol. 37, no. 22, pp. 5271.
48. M. R. Querry, Optical Constants. *MISSOURI UNIV-KANSAS CITY*, 1985.
49. S. Farooq and R. E. de Araujo, Engineering a Localized Surface Plasmon Resonance Platform for Molecular Biosensing, *OJAppS*, 2018, vol. 8, no. 3, pp. 126–139.
50. M. N. Kholodtsova, P. V. Grachev, W. C. Blondel, et al., Application of devices for space-resolved spectroscopy on the example of two-layer phantoms containing metallic nanoparticles, *Biomedical Photonics*, 2018, vol. 7, no. 2, pp. 4–12.
51. G. Baffou, R. Quidant, and F. J. García de Abajo, Nanoscale Control of Optical Heating in Complex Plasmonic Systems, *ACS Nano*, 2010, vol. 4, no. 2, pp. 709–716.
52. E. Cazares-Cortes, S. Cabana, C. Boitard, et al., Recent insights in magnetic hyperthermia: From the "hot-spot" effect for local delivery to combined magneto-photo-thermia using magneto-plasmonic hybrids, *Advanced Drug Delivery Reviews*, 2019, vol. 138, pp. 233–246.
53. J. Dong and J. I. Zink, Taking the Temperature of the Interiors of Magnetically Heated Nanoparticles, *ACS Nano*, 2014, vol. 8, no. 5, pp. 5199–5207.
54. D. Gareau, A. Desrosiers, and A. Vallée-Bélisle, Programmable Quantitative DNA Nanothermometers, *Nano Lett*, 2016, vol. 16, no. 7, pp. 3976–3981.
55. A. Riedinger, P. Guardia, A. Curcio, et al., Subnanometer Local Temperature Probing and Remotely Controlled Drug Release Based on Azo-Functionalized Iron Oxide Nanoparticles, *Nano Lett*, 2013, vol. 13, no. 6, pp. 2399–2406.

Photothermal Therapy and MR Imaging//Nanotheranostics. – 2018. – Vol. 2 (2). – P. 106–116.

35. Cabana S., Curcio A., Michel A., Wilhelm C., and Abou-Hassan A. Iron Oxide Mediated Photothermal Therapy in the Second Biological Window: A Comparative Study between Magnetite/Maghemite Nanospheres and Nanoflowers//Nanomaterials. – 2020. – Vol.10 (8). – P.1548.
36. Shi J., Yu X., Wang L., Liu Y. et al. PEGylated fullerene/iron oxide nanocomposites for photodynamic therapy, targeted drug delivery and MR imaging//Biomaterials. – 2013. – Vol. 34 (37). – P. 9666–9677.
37. Penon O., Marín M. J., Amabilino D. B., Russell D. A. and Pérez-García L. Iron oxide nanoparticles functionalized with novel hydrophobic and hydrophilic porphyrins as potential agents for photodynamic therapy//Journal of Colloid and Interface Science. – 2016. – Vol. 462. – P. 154–165.
38. Климов В. В., Наноплазмоника//2nd ed. Физматлит. – 2010.
39. Bashevoy M. V., Fedotov V. A., and Zheludev N. I. Optical whirlpool on an absorbing metallic nanoparticle//Opt. Express. – 2005. – Vol. 13 (21). – P. 8372.
40. Sharma S. K., Shrivastava N., Rossi F. et al. Nanoparticles-based magnetic and photo induced hyperthermia for cancer treatment//Nano Today. – 2019. – Vol. 29. – P. 100795.
41. Lozano-Pedraza C., Plaza-Mayoral E., Espinosa A., Sot B., et al. Assessing the parameters modulating optical losses of iron oxide nanoparticles under near infrared irradiation//Nanoscale Adv. – 2021. – Vol. 3 (22). – P. 6490–6502.
42. Jeong Y., Kook Y.-M., Lee K., and Koh W.-G. Metal enhanced fluorescence (MEF) for biosensors: General approaches and a review of recent developments//Biosensors and Bioelectronics. – 2018. – Vol. 111. – P. 102–116.
43. M. M. Sigalas, D. A. Fattal, R. S. Williams, et al., Electric field enhancement between two Si microdisks//Opt. Express. – 2007. – Vol. 15 (22). – P. 14711.
44. S. Toroghi and P. G. Kik, Photothermal response enhancement in heterogeneous plasmon-resonant nanoparticle trimmers//Phys. Rev. B. – 2014. – Vol. 90 (20). – P. 205414.
45. N. G. Khlebtsov, T-matrix method in plasmonics: An overview//Journal of Quantitative Spectroscopy and Radiative Transfer. – 2013. – Vol. 123. – P. 184–217.
46. D. W. Mackowski and M. I. Mishchenko, A multiple sphere T-matrix Fortran code for use on parallel computer clusters//Journal of Quantitative Spectroscopy and Radiative Transfer. – 2011. – Vol. 112 (13). – P. 2182–2192.
47. A. D. Rakić, A. B. Djurišić, J. M. Elazar, and M. L. Majewski, "Optical properties of metallic films for vertical-cavity optoelectronic devices//Appl. Opt. – 1998. – Vol. 37 (22). – P. 5271.
48. M. R. Querry, Optical Constants//MISSOURI UNIV-KANSAS CITY. – 1985.
49. S. Farooq and R. E. de Araujo, Engineering a Localized Surface Plasmon Resonance Platform for Molecular Biosensing//OJAppS. – 2018. – Vol. 08 (03). – P. 126–139.
50. Kholodtsova M. N., Grachev P. V., W. Blondel C. et al., Application of devices for space-resolved spectroscopy on the example of two-layer phantoms containing metallic nanoparticles//Biomedical Photonics. – 2018. – Vol. 7 (2). – P. 4–12.
51. Baffou G., Quidant R., and García de Abajo F. J. Nanoscale Control of Optical Heating in Complex Plasmonic Systems//ACS Nano. – 2010. – Vol. 4 (2). – P. 709–716.
52. Cazares-Cortes E., Cabana S., Boitard C. et al., Recent insights in magnetic hyperthermia: From the "hot-spot" effect for local delivery to combined magneto-photo-thermia using magneto-plasmonic hybrids//Advanced Drug Delivery Reviews. – 2019. – Vol. 138. – P. 233–246.
53. Dong J. and Zink J. I. Taking the Temperature of the Interiors of Magnetically Heated Nanoparticles//ACS Nano. – 2014. – Vol. 8 (5). – P. 5199–5207.

56. C. Joyce, S. M. Fothergill, F. Xie, Recent advances in gold-based metal enhanced fluorescence platforms for diagnosis and imaging in the near-infrared, *Materials Today Advances*, 2020, vol. 7, pp. 100073.
57. Ángela I. López-Lorente, Recent developments on gold nanostructures for surface enhanced Raman spectroscopy: Particle shape, substrates and analytical applications, *A review, Analytica Chimica Acta*, 2021, vol. 1168, pp. 338474.
58. Sajid Farooq, Renato E. de Araujo, dentifying high performance gold nanoshells for singlet oxygen generation enhancement, *Photodiagnosis and Photodynamic Therapy*, 2021, vol. 35, pp. 102466.
59. Seyfollah Toroghi and Pieter G. Kik Cascaded plasmon resonant field enhancement in nanoparticle dimers in the point dipole limit Appl, *Phys. Lett*, 2013, vol. 100, pp. 183105.
60. Davletshin Y. R., Kumaradas J. C., *J. Beilstein Nanotechnol*, 2016, vol. 7, pp. 869–880. doi:10.3762/bjnano.7.79

54. Gareau D., Desrosiers A., and Vallée-Bélisle A. Programmable Quantitative DNA Nanothermometers//Nano Lett. – 2016. – Vol. 16 (7). – P. 3976–3981.
55. Riedinger A., Guardia P., Curcio A. et al., Subnanometer Local Temperature Probing and Remotely Controlled Drug Release Based on Azo-Functionalized Iron Oxide Nanoparticles//Nano Lett. – 2013. – Vol. 13 (6). – P. 2399–2406.
56. Joyce C., Fothergill S. M., Xie F. Recent advances in gold-based metal enhanced fluorescence platforms for diagnosis and imaging in the near-infrared//Materials Today Advances. – 2020. – Vol. 7. – P. 100073.
57. Ángela I. López-Lorente, Recent developments on gold nanostructures for surface enhanced Raman spectroscopy: Particle shape, substrates and analytical applications//A review, Analytica Chimica Acta. – 2021. – Vol. 1168. – P. 338474.
58. Sajid Farooq, Renato E. de Araujo, dentifying high performance gold nanoshells for singlet oxygen generation enhancement//Photodiagnosis and Photodynamic Therapy. – 2021. – Vol. 35. – P. 102466.
59. Seyfollah Toroghi and Pieter G. Kik Cascaded plasmon resonant field enhancement in nanoparticle dimers in the point dipole limit Appl//Phys. Lett. – 2013. – Vol. 100. – P. 183105.
60. Y. R. Davletshin, J. C. Kumaradas, J. Beilstein Nanotechnol. – 2016. – Vol. 7. – P. 869–880. doi:10.3762/bjnano.7.79